Newton

Article

Certifying the quantumness of a nuclear spin qudit through its uniform precession

Highlights

- The quantumness of a spin state can be certified by measuring its precession
- Exotic states of an antimony nuclear spin are certified quantum by this method
- The key requirement is measuring the positivity instead of the spin projection
- The method is resource efficient and may find widespread application

Authors

Arjen Vaartjes, Martin Nurizzo, Lin Htoo Zaw, ..., David N. Jamieson, Valerio Scarani, Andrea Morello

Correspondence

a.morello@unsw.edu.au

In brief

It is widely believed that the quantum mechanical precession of a spin behaves similarly to the precession of a classical gyroscope. In this work, Vaartjes et al. show that in high-dimensional spins such as antimony in silicon, it is possible to prove the quantumness of exotic spin states by monitoring their precession.

Vaartjes et al., 2025, Newton *1*, 100017
March 3, 2025
https://doi.org/10.1016/j.newton.2025.100017

CellPress

Please cite this article in press as: Vaartjes et al., Certifying the quantumness of a nuclear spin qudit through its uniform precession, Newton (2025), https://doi.org/10.1016/j.newton.2025.100017

Newton

CellPress
OPEN ACCESS

Article

Certifying the quantumness of a nuclear spin qudit through its uniform precession

Arjen Vaartjes,[1,2] Martin Nurizzo,[1,2] Lin Htoo Zaw,[3] Benjamin Wilhelm,[1,2] Xi Yu,[1,2] Danielle Holmes,[1,2] Daniel Schwienbacher,[1,2] Anders Kringhøj,[1,2] Mark R. van Blankenstein,[1,2] Alexander M. Jakob,[2,4] Fay E. Hudson,[1,5] Kohei M. Itoh,[6] Riley J. Murray,[7] Robin Blume-Kohout,[8] Namit Anand,[9,10] Andrew S. Dzurak,[1,5] David N. Jamieson,[2,4] Valerio Scarani,[3,11] and Andrea Morello[1,2,12,*]

[1]School of Electrical Engineering and Telecommunications, UNSW Sydney, Sydney, NSW 2052, Australia
[2]Australian Research Council Centre for Quantum Computation and Communication Technology, University of New South Wales, Sydney, NSW, Australia
[3]Centre for Quantum Technologies, National University of Singapore, 3 Science Drive 2, Singapore 117543, Singapore
[4]School of Physics, University of Melbourne, Melbourne, VIC 3010, Australia
[5]Diraq Pty. Ltd., Sydney, NSW, Australia
[6]School of Fundamental Science and Technology, Keio University, Kohoku-ku, Yokohama, Japan
[7]Quantum Performance Laboratory, Sandia National Laboratories, Livermore, CA 94550, USA
[8]Quantum Performance Laboratory, Sandia National Laboratories, Albuquerque, NM 87185, USA
[9]Quantum Artificial Intelligence Laboratory (QuAIL), NASA Ames Research Center, Moffett Field, CA 94035, USA
[10]KBR, Inc., 601 Jefferson Street, Houston, TX 77002, USA
[11]Department of Physics, National University of Singapore, 2 Science Drive 3, Singapore 117542, Singapore
[12]Lead contact
*Correspondence: a.morello@unsw.edu.au
https://doi.org/10.1016/j.newton.2025.100017

ACCESSIBLE OVERVIEW It is widely believed that the quantum mechanical precession of a spin behaves similarly to the precession of a classical gyroscope. Contrary to this conventional wisdom, the present work highlights that such similarity only holds in special circumstances, such as two-dimensional spins (qubits) or semi-classical states of larger spins. The work proposes a simple protocol that enables the quantumness of a spin system to be determined through measurements of its precession. The protocol is experimentally demonstrated on the nuclear spin of a single antimony atom, implanted in a silicon nanoelectronic device. The results show significant deviations from those expected from classical systems. Such a means to certify nonclassical states could be of interest for many applications, including quantum information processing, quantum sensing and quantum foundations.

SUMMARY

Spin precession is a textbook example of the dynamics of a quantum system that exactly mimics its classical counterpart. Here, we challenge this view by certifying the quantumness of exotic states of a nuclear spin through its uniform precession. The key to this result is measuring the positivity, instead of the expectation value, of the x-projection of the precessing spin, and using a spin >1/2 qudit that is not restricted to semi-classical spin coherent states. The experiment is performed on a single spin-7/2 ^{123}Sb nucleus, implanted in a silicon nanoelectronic device, amenable to high-fidelity preparation, control, and projective single-shot readout. Using Schrödinger cat states and other bespoke states of the nucleus, we violate the classical bound by 18 standard deviations, proving that no classical probability distribution can explain the statistic of this spin precession and highlighting our ability to prepare quantum resource states with high fidelity in a single-atomic-scale qudit.

INTRODUCTION

Drawing the boundary between classical and quantum behavior has been a long-standing challenge, especially for single-particle systems. The spin-1/2 particle, a textbook example of a quantum system, illustrates this difficulty. Undergraduate physics students learn that the spin of an electron is quantized: the Stern-Gerlach experiment shows that, upon measuring the orientation of the spin, only one of two discrete possibilities can be observed. However, they soon after learn about the

Please cite this article in press as: Vaartjes et al., Certifying the quantumness of a nuclear spin qudit through its uniform precession, Newton (2025), https://doi.org/10.1016/j.newton.2025.100017

Ehrenfest theorem, which states that the time dependence of the expectation values of dynamical variables are identical for classical and quantum systems with Hamiltonians that are up to quadratic in position and momentum, or equivalently, up to linear in angular momenta.[1] Magnetic resonance textbooks invariably start by showing that the quantum mechanical treatment of a precessing spin yields the same result as the precession of a classical angular momentum,[2] leaving many students with the impression that there is nothing quantum about spin precession.

The key point here—seldom made explicit by standard textbooks, but crucial to our discussion—is that the classical-like behavior of spin-1/2 particles stems from their limited Hilbert space dimension ($d = 2$), which can only accommodate semi-classical spin-coherent states,[3,4] and imposes a statistical behavior explainable by noncontextual hidden-variable models.[5] Therefore, higher spins with $d \geq 3$ are required to observe quantum behaviors that cannot be mimicked by classical analogs.[6–8]

Even using physical systems with enough complexity and Hilbert space dimension to support nonclassical states, detecting their quantumness is a delicate task. Conventional approaches have typically relied on measuring correlations between observables using, for instance, Bell nonlocality tests,[9] Kochen-Specker noncontextuality tests,[7] and Leggett-Garg inequality tests.[10] However, these methods have limitations. Bell nonlocality only probes multipartite notions of quantumness and thus cannot test the nonclassicality of a single particle. Single-particle tests like Kochen-Specker noncontextuality and Leggett-Garg inequalities require simultaneous or sequential measurements, together with assumptions that are virtually untestable (e.g., two measurements commute exactly,[11] the system has no classical memory,[12] a classical system was measured noninvasively[13]). Other proposed indicators of nonclassicality like Wigner negativity[14] not only require full or partial tomography, but might not have a clear interpretation in finite-dimensional spin systems.[15] Alternative approaches include evolving the system with higher-order Hamiltonians thought to be needed to overcome the classicality of linear dynamics.[4]

Here, we present the first experimental demonstration of a protocol to detect the quantumness of a spin state via measurements of its precession. Inspired by Tsirelson's work on harmonic oscillators[16] and later extended to spin systems by Zaw et al.,[17] this protocol challenges conventional wisdom by revealing clear quantum signatures in a system undergoing uniform precession, despite Ehrenfest's theorem suggesting classical-like average behavior. The success of the protocol formally disproves the existence of a classical joint probability distribution that could explain the observed statistics, which is a key indicator of nonclassicality.[18]

The protocol is remarkably simple to implement. It operates under the sole assumption that the measured observable undergoes a uniform precession (i.e., at constant angular velocity) in some suitably defined reference frame. This can readily be implemented in qudits by utilizing recently demonstrated spin-coherent control techniques.[19–21] Furthermore, no simultaneous or sequential measurements are required and, for a spin of size I, only $2I$ measurements of dichotomic observables are required to detect nonclassicality with the precession protocol, compared to $5(2I+1)$ measurements of $(2I+1)$ outcome observables to tomograph the state efficiently.[22,23]

In this work, we implement the precession protocol on a single spin-7/2 ^{123}Sb nucleus implanted within a silicon nanoelectronic device. We initialize non-classical states and observe significant violations of the classical bound in the protocol measurements. These violations are possible due to the high fidelity of our prepared states, which we verify with quantum state tomography. Furthermore, we also achieve a score close to the general theory-independent maximum possible in a spin-3/2 subspace, which rules out alternatives to quantum theory that cannot reach the same value.[24] We first present the protocol and its implementation, and leave for the end the discussion as to why it works despite widely held beliefs on the implications of the Ehrenfest theorem or textbook proofs that spin precession follows the classical dynamics.[2]

RESULTS

Classical protocol

To illustrate the classical variant of the protocol, we consider the angular momentum $\underline{L} = \{L_x, L_y, L_z\}$ of a classical gyroscope precessing around the z axis with a frequency ω, and a precession angle defined as $\varphi(t) = \omega t + \varphi_0$ (see Figure 1A), where φ_0 denotes the initial offset angle. The coordinates L_x and L_y of the gyroscope evolve according to the equations of motion:

$$\begin{aligned} L_x(t) &= L_x(0)\cos\varphi(t) + L_y(0)\sin\varphi(t), \\ L_y(t) &= L_y(0)\cos\varphi(t) + L_x(0)\sin\varphi(t). \end{aligned} \qquad \text{(Equation 1)}$$

The protocol involves segmenting one precession period into K equally separated times ($K = 7$ in Figure 1A). At each of these, we measure the positivity of the L_x-coordinate (Figure 1B):

$$\mathrm{Pos}(L_x) = \begin{cases} 1 & \text{if } L_x \geq 0 \\ 0 & \text{otherwise.} \end{cases} \qquad \text{(Equation 2)}$$

The classical score, P_K^c is defined as the expectation value of $\mathrm{Pos}(L_x)$ over one precession period divided into K equal time intervals:

$$P_K^c = 1/K \sum_{k=1}^{K} \mathrm{Pos}\left(L_x\left(\frac{2\pi k}{\omega K} + \phi_0\right)\right). \qquad \text{(Equation 3)}$$

In the example, out of 7 intervals, the x-coordinate is positive 4 times, resulting in a classical score of $P_7^c = 4/7$.

The score P_K^c is dependent on the initial state parameterized by φ_0—in other words, P_7^c is either 3/7 when the state starts in a gray region or 4/7 when it starts in a yellow region, as depicted in Figure 1C. We define the classical bound $\mathbf{P_K^c}$ as the maximum classical score, which is obtained by maximizing over all possible initial states.

Quantum protocol

For the quantum version of the protocol, we consider the spin vector $\vec{\hat{I}} = \{\hat{I}_x, \hat{I}_y, \hat{I}_z\}$ as a quantum analog to classical angular momentum. Under a constant $\hat{I}_z$ term in the Hamiltonian, the spin

Please cite this article in press as: Vaartjes et al., Certifying the quantumness of a nuclear spin qudit through its uniform precession, Newton (2025), https://doi.org/10.1016/j.newton.2025.100017

CellPress
OPEN ACCESS

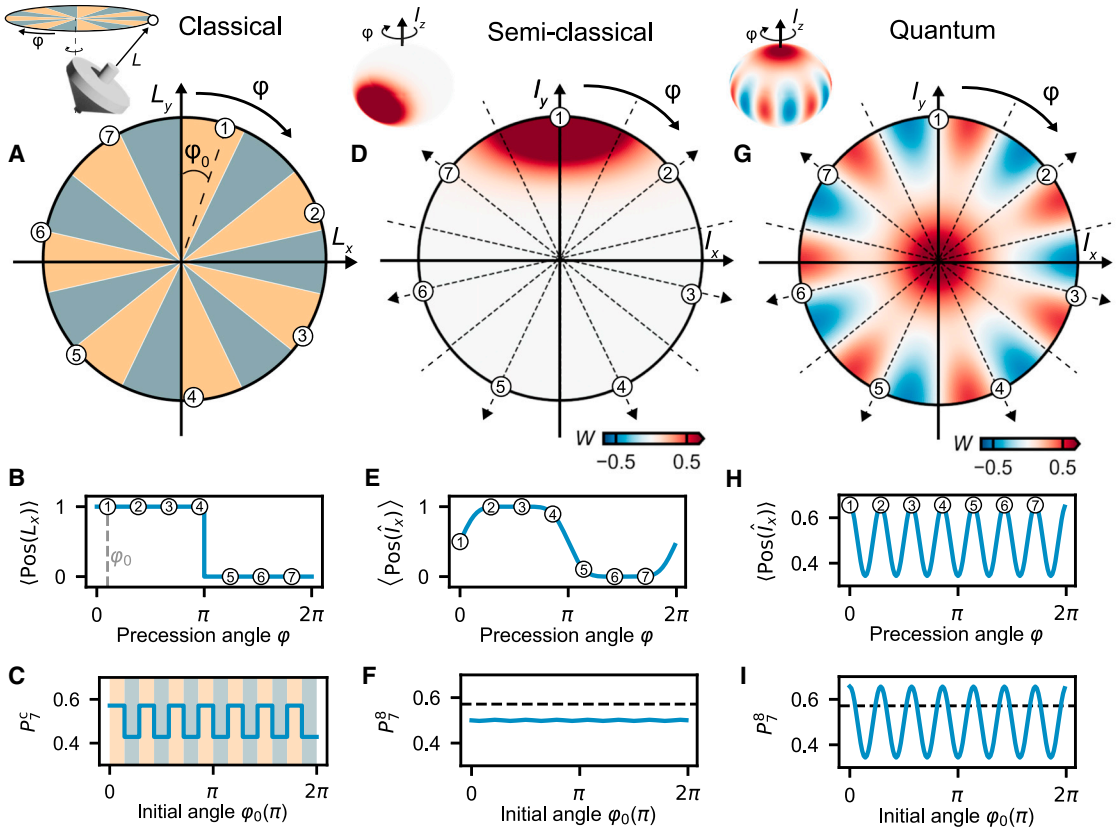

Figure 1. Quantumness detection protocol for uniformly precessing spin in classical, semi-classical, and quantum states

(A) Phase space representation of the uniform precession protocol for a classical precessing gyroscope. A precession period is divided into K equal angles. The numbered dots indicate a possible set of $K = 7$ equidistantly sampled angles in one precession period. Yellow (gray) regions indicate the initial angles φ_0 that maximize (minimize) the classical score.

(B) Expectation value of the positivity of L_x, as a function of the precession angle φ. The numbered dots show $K = 7$ sampled angles, corresponding to (A).

(C) Classical score of the protocol P_7^{cl} for $K = 7$, as a function of the initial angular shift φ_0. P_K^{cl} is the mean over the K sampled points. The yellow (gray) regions correspond with the yellow (gray) areas in (A) and indicate the initial angles for which the classical score is maximum (minimum). For $K = 7$, the maximum classical score is $P_K^{cl} = 4/7 = 0.571$.

(D) The Wigner function of a spin-7/2 spin-coherent state oriented along the y axis (inset), with its polar projection for polar angles $\theta \in [0, \pi/2]$. The Wigner function undergoes a rotation around the z axis. The rotation is again split up in $K = 7$ equal angles (numbered dots).

(E) Expectation value of the positivity of the $\hat{I}_x$ operator and a possible set of $K = 7$ equidistant angles (numbered dots).

(F) The quantum score P_7^8 as a function of the initial angle. Note that the semi-classical spin-coherent state does not violate the classical bound (dashed line).

(G) The Wigner function of a spin-7/2 cat state (inset) and its polar projection for $\theta \in [0, \pi/2]$.

(H) The expectation value of $\mathrm{Pos}(\hat{I}_x)$ shows $d - 1 = 7$ oscillation periods, corresponding to the interference pattern along φ of the Wigner function. The numbers indicate the set of $K = 7$ angles that maximize the quantum score P_7^8.

(I) P_7^8 as a function of the initial shift φ_0. The maximum quantum score $P_7^8 = 0.656$ violates the classical bound (dashed line).

precesses uniformly in the $\hat{I}_x$-$\hat{I}_y$ plane according to the same equations of motion as the classical case (Equation 1), with $L_x \mapsto \hat{I}_x$ and $L_y \mapsto \hat{I}_y$.

Furthermore, the probability of detecting a positive component of $\hat{I}_x$ becomes an operator, $\mathrm{Pos}(x) \mapsto \mathrm{Pos}(\hat{I}_x)$, defined as:

$$\mathrm{Pos}(\hat{I}_x) = \frac{1}{2}[\mathbb{I} + \mathrm{sgn}(\hat{I}_x)], \qquad \text{(Equation 4)}$$

where II is the identity matrix and the sign operator is defined as

$$\mathrm{sgn}(\hat{I}_x) = \sum_{m=-I}^{I} \mathrm{sgn}(m)|m_x\rangle\langle m_x|, \qquad \text{(Equation 5)}$$

where $|m_x\rangle$ are the eigenstates of $\hat{I}_x$. Then, for a pure quantum state $|\psi\rangle$ in a d-dimensional Hilbert space, the quantum score P_K^d is determined by measuring the expectation value $\langle \mathrm{Pos}(\hat{I}_x)\rangle$ at K separate times during one precession period around the $\hat{I}_z$ axis:

$$P_K^d = \frac{1}{K}\sum_{k=1}^{K} \langle\psi_k|\mathrm{Pos}(\hat{I}_x)|\psi_k\rangle, \qquad \text{(Equation 6)}$$

where $|\psi_k\rangle = e^{i(2\pi k/K)\hat{I}_z}|\psi\rangle$ is the rotated initial state. The maximum quantum score is $\mathbf{P_k^d}$ achieved by maximizing over all initial states $|\psi\rangle$.

Please cite this article in press as: Vaartjes et al., Certifying the quantumness of a nuclear spin qudit through its uniform precession, Newton (2025), https://doi.org/10.1016/j.newton.2025.100017

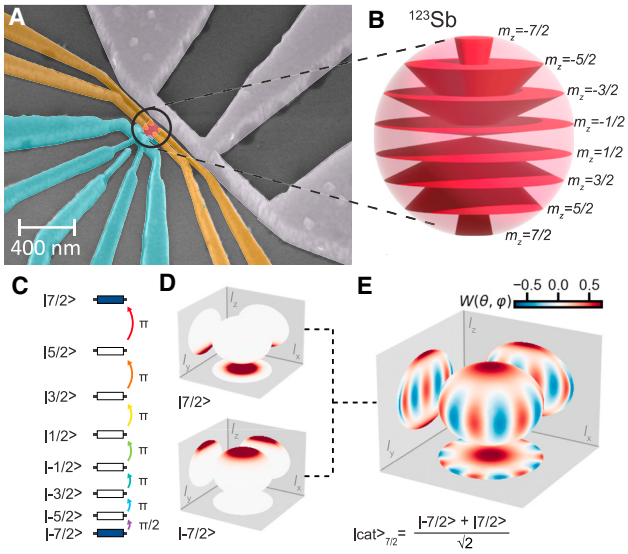

Figure 2. Preparation of non-classical states of a ^{123}Sb nucleus in a silicon device

(A) Scanning electron micrograph of a device identical to that used in this experiment. The ion-implanted^{123} Sb nucleus is located in the donor implant window (red). The electrostatic donor gates (yellow), single electron transistor (teal) and microwave antenna (light gray) are shown.

(B) Spin angular momentum states of the^{123} Sb nucleus under an external magnetic field, showing 8 different quantum levels m_z of the nucleus.

(C) State initialization process, using ladder operations (Givens rotations) to create a spin-cat state: a sequence of $\pi/2$ and π pulses (ordered bottom to top) drive transitions between different $|m_I\rangle$ eigenstates of the $\hat{I}_z$-operator.

(D) Three-dimensional visualization of the spin-Wigner function $W(\theta,\phi)$ for the spin-coherent eigenstates $|7/2\rangle$ and $|-7/2\rangle$.

(E) Spin-Wigner function $W(\theta,\varphi)$ (supplemental information, Note S1.5) of the cat state $|-7/2\rangle - |-7/2\rangle/\sqrt{2}$, illustrating the interference fringes characteristic of a non-classical spin-cat state.

Only a subset of quantum states breaks the classical bound.[24] We illustrate this in Figures 1D–1I with two examples on an 8-dimensional spin-7/2 system: the semi-classical spin-coherent state defined as the minimum-uncertainty state pointing along the y axis[3] and the quantum spin-cat state defined as the superposition of two maximally separated spin coherent states along the z axis ($|\text{cat}_{7/2}\rangle_z = (|7/2\rangle - |-7/2\rangle)/\sqrt{2}$).[19,25]

For the spin-coherent state (Figure 1D), the Wigner quasi-probability distribution (see Note S1.5) is concentrated in one spot of the phase space, qualitatively resembling classical behavior. However, unlike the classical case for which the probability distribution is an infinitesimally small point, its Wigner function spreads out as a Gaussian distribution due to the uncertainty principle ($\delta\hat{I}_x\delta\hat{I}_y \geq |\hat{I}_z|/2$). Despite being a pure quantum state, this state does not break the classical bound. For this state, $\langle \text{Pos}(\hat{I}_x)\rangle$ (Figure 1E) appears as a smoothed version of the classical case (Figure 1B), with the phase space blob essentially acting as a Gaussian filter in the φ direction.

In contrast, the quantum spin-cat state $|\text{cat}_{7/2}\rangle_z$ exhibits non-classical behavior. Its Wigner function is not concentrated in a single region but is spread out over multiple spots in the phase space, showing a distinct interference pattern along the φ direction. The expectation value for the positivity operator $\langle \text{Pos}(\hat{I}_x)\rangle$ displays a corresponding oscillation pattern with 7 peaks and 7 valleys. When the $K = 7$ equally separated angles are exactly matching the peaks of the oscillation, the quantum score P_7^8 is maximized and the classical bound is violated. This implies that the observations could not have arisen from a classical joint probability distribution of I_x and I_y, which certifies the quantumness of the spin-cat state.

Experimental realization

We performed the uniform precession protocol on a single ionized $^{123}Sb^+$ donor implanted into a silicon chip.[26] The nuclear spin $I = 7/2$ gives rise to an 8-dimensional Hilbert space, described by the following static spin Hamiltonian in frequency units:

$$\hat{\mathcal{H}}_{D^+} = -\gamma_n B_0 \hat{I}_z + \sum_{\alpha,\beta \in \{x,y,z\}} Q_{\alpha\beta}\hat{I}_\alpha\hat{I}_\beta, \qquad \text{(Equation 7)}$$

where $B_0 = 1.384$ T is a static magnetic field, $\gamma_n = 5.55$ MHz/T is the nuclear gyromagnetic ratio, $\hat{I}_{\{x,y,z\}}$ are the nuclear spin operators, and $Q_{\alpha\beta}$ is the quadrupole strength, which allows for individual addressability.[26,27] The coupling between the 8 different eigenstates is generated on demand by oscillating magnetic fields created via an on-chip antenna. This interaction can induce nuclear magnetic resonance (NMR) transitions and is described by the following interaction Hamiltonian:

$$\hat{\mathcal{H}}_1(t) = -\gamma_n \hat{I}_x \sum_{i=0}^{2I-1} \cos(2\pi f_i t + \phi_i) B_{1,i}(t), \qquad \text{(Equation 8)}$$

where f_k are the NMR frequencies ($f_0 = \langle -7/2|\hat{\mathcal{H}}_{D^+}|-7/2\rangle - \langle -5/2|\hat{\mathcal{H}}_{D^+}|-5/2\rangle$, etc.), $B_{1,i}(t)$ the oscillating magnetic field amplitudes, and φ_i the phases. The dynamics of the qudit is conveniently described in a generalized rotating frame (GRF),[19,28,29] which changes the basis to the rotating eigenstates $|m_z'\rangle = \exp(-i2\pi E_m t/\hbar)|m_z\rangle$, where E_m are the eigenenergies of the static Hamiltonian.[30] In this basis, the Hamiltonian is transformed into

$$\hat{\mathcal{H}}_G = \begin{pmatrix} 0 & g_0 e^{i\varphi_0} & 0 & \cdots & 0 & 0 \\ g_0^* e^{-i\varphi_0} & 0 & g_1 e^{i\varphi_1} & \cdots & 0 & 0 \\ 0 & g_1^* e^{-i\varphi_1} & 0 & \cdots & 0 & 0 \\ \vdots & \vdots & \vdots & \ddots & \vdots & \vdots \\ 0 & 0 & 0 & \cdots & 0 & g_6 e^{i\varphi_6} \\ 0 & 0 & 0 & \cdots & g_6^* e^{-i\varphi_6} & 0 \end{pmatrix}, \qquad \text{(Equation 9)}$$

where $g_i = -\frac{\gamma_n}{4} B_{1,i}(t)\langle -7/2 + i|\hat{I}_x|-7/2 + (i+1)\rangle$.

This Hamiltonian outlines the experimental tools for the precession protocol. State initialization is performed (see supplemental methods, section 2) with two-level ladder operations or Givens rotations,[31] with sequentially applied single-tone drives, activating only one $B_{1,i}$ at a time. Figure 2C shows the example

Please cite this article in press as: Vaartjes et al., Certifying the quantumness of a nuclear spin qudit through its uniform precession, Newton (2025), https://doi.org/10.1016/j.newton.2025.100017

CellPress
OPEN ACCESS

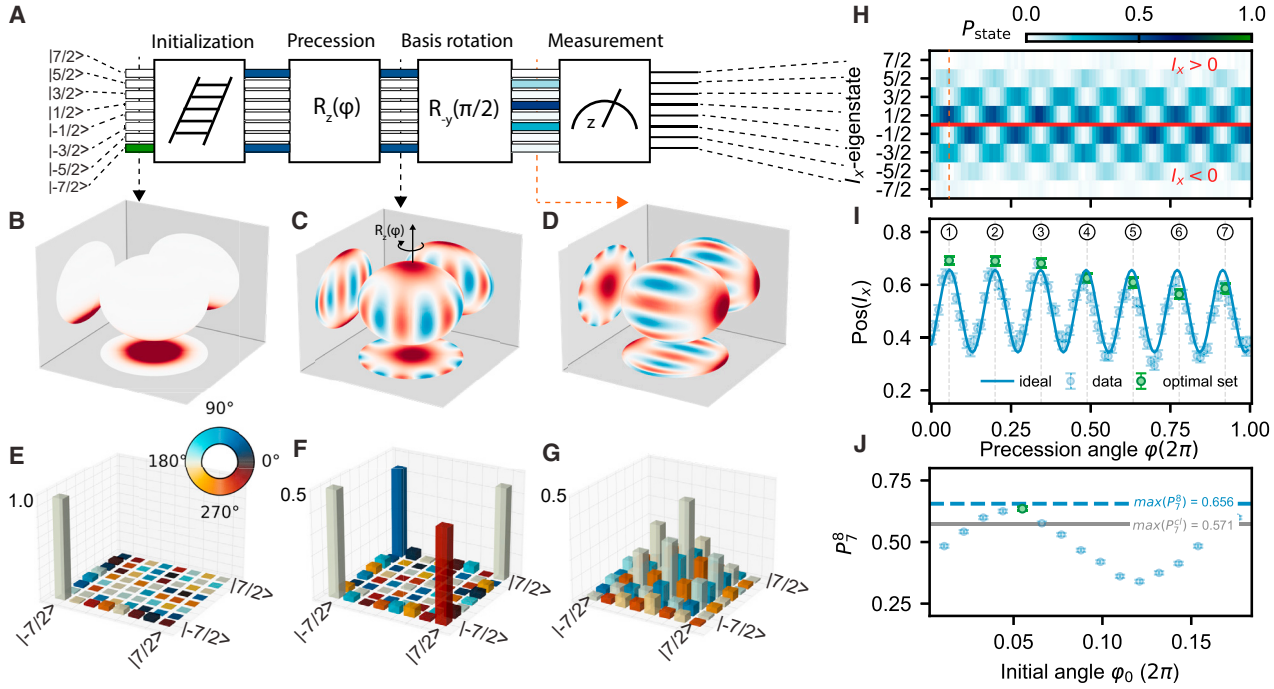

Figure 3. Experimental realization of the protocol for detecting quantumness in uniform precession

(A) The sequence of operations in the protocol: initialization, precession, basis rotation, and measurement. Initialization is achieved through ladder operations to prepare the nucleus in a specific state. During precession, the state rotates around the z axis by an angle φ. Basis rotation is performed using an SU(2) $\pi/2$ rotation around the $-y$ axis, followed by measurement in the z basis. The bar colors in the pulse sequence represent state probabilities at each protocol step, with the same color scale as (H), and the colors before the measurement correspond to the line cut (orange dashed line) in (H).

(B–D) Experimentally reconstructed Wigner functions show the state evolution throughout the protocol, obtained via quantum state tomography (see supplemental information, Note S2.1).

(E–G) Density matrices corresponding to the Wigner plots.

(H) Populations of the $\hat{I}_x$-eigenstates $|m_x\rangle$ as a function of the precession angle φ. The populations are inferred from the probabilities of measuring the $|m_z\rangle$ states after the basis rotation. The red horizontal line separates positive from negative eigenstates. The orange dashed vertical line indicates the angle φ for which the populations in (A) and the Wigner function in (D) are displayed.

(I) The expectation value of the positivity operator $\mathrm{Pos}(\hat{I}_x)$ (blue data points) shows oscillations in φ, closely matching the simulated ideal behavior (blue solid line) of a spin-cat state. The numbered green data points indicate the optimal set of $K = 7$ equally separated points that maximize the measured quantum score in the protocol.

(J) The highest measured quantum score for $d = 8$ and $K = 7$, $P_7^8 = 0.636(7)$, approaches the theoretical maximum quantum score $\mathbf{P}_7^8 = 0.656$ and exceeds the classical bound $\mathbf{P}_7^c = 0.571$ by 18 standard deviations. The error bars in (I) and (J) represent 2σ confidence intervals.

Figure360

Figure360▷ For a Figure360 author presentation of Figure 3, see https://doi.org/10.1016/j.newton.2025.100017#mmc2.

of preparing the spin-cat state $|\mathrm{cat}_{7/2}\rangle_z$. Furthermore, any state can be rigidly rotated by SU(2)-covariant rotations, produced by driving all NMR transitions with tones of equal amplitude $B_{1,i} = B_1$.[19] Finally, the uniform precession required for the protocol is implemented through the virtual selective number arbitrary phase gates. When applied with a specific set of phases, these gates generate virtual $\hat{I}_z$ rotations. Here, these rotations are achieved by updating the GRF through equal phase shifts of all 7 reference clocks by φ. A detailed description of and a demonstration on the spin-coherent state are given in supplemental methods, section 3.

Pulse sequence

The protocol is summarized by the following 4-step pulse sequence on the ground state $|-7/2\rangle$ (Figure 3A):

(1) Initialize the desired state using 2-level ladder operations.
(2) Emulate uniform precession around the $\hat{I}_z$ axis by performing an R_z rotation with angle φ.
(3) Perform a $\pi/2$ SU(2) rotation around the $-y$ axis to change the measurement basis from $\hat{I}_z$ to $\hat{I}_x$.
(4) Measure the state populations in the $\hat{I}_z$-basis.

This sequence allows us to measure $\mathrm{Pos}(\hat{I}_x)$ at K angles φ_k and determine a quantum score P_K^d.

Breaking the classical bound with spin-cat states

The Schrödinger cat state—a paradigmatic example of a nonclassical state, and a useful resource in quantum error correction[32–34] and quantum sensing[35,36]—is a particularly suitable state on which to test this protocol. Figure 3 demonstrates the breaking of the classical bound using the largest cat state,

Please cite this article in press as: Vaartjes et al., Certifying the quantumness of a nuclear spin qudit through its uniform precession, Newton (2025), https://doi.org/10.1016/j.newton.2025.100017

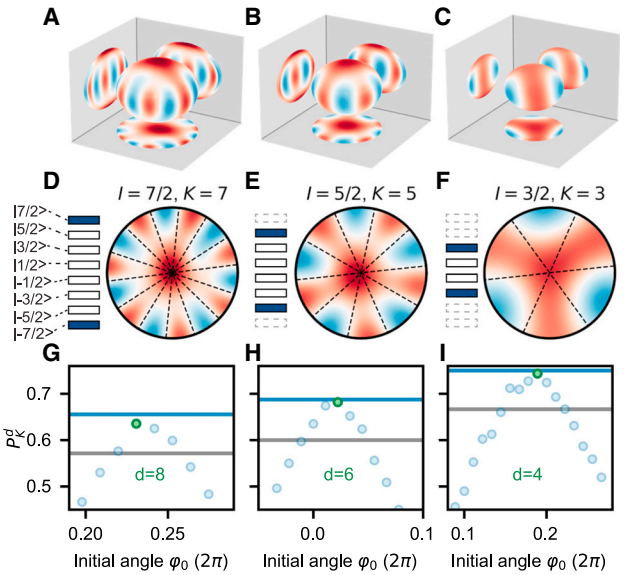

Figure 4. Breaking the classical bound in different size subspaces

(A–C) Reconstructed Wigner functions of the spin-cat states in (A) $d = 8$, (B) $d = 6$, and (C) $d = 4$. The size of the sphere reflects the size of the subspace. The Wigner spheres are reconstructed from full 8-dimensional quantum state tomography (see supplemental information, Note S2.1).

(D–F) Population distribution (bars at left) and polar projection (right) of the spin-cat states. (D) The $d = 8$ cat state occupies the whole Hilbert space of the ^{123}Sb nucleus. (E) The $d = 6$ cat state is spanned by the $|\pm 5/2\rangle$ states. (F) The $d = 4$ cat state is the superposition of the $|\pm 3/2\rangle$ states.

(G–I) The measured quantum scores P_k^d (blue data points) exceed the classical bound for a small range of initial angles φ_0. The optimal measured quantum score (green dot) approaches the theoretical maximum (blue horizontal line) and violates the classical bound (gray horizontal line) for all even $d > 3$.

$|\mathrm{cat}_{7/2}\rangle_z$.[17] By selecting $K = 7$ equidistant points along the φ axis and averaging the values of $\mathrm{Pos}(\hat{I}_x)$ at these points, we obtain a quantum score $P_7^8 = 0.636(7)$ (throughout this work, the error represents a 2σ confidence interval). This is an observed violation of the classical bound by 18 standard deviations, which certifies the quantumness of state we prepared on the ^{123}Sb nuclear spin.

Such a large violation must mean that we were able to prepare $|\mathrm{cat}_{7/2}\rangle_z$ with a high fidelity. Indeed, we can quantitatively define a lower bound of the fidelity with the observed score as $\mathcal{F} \geq 16(2P_7^8 - 1)/5 = 87\%$ (see Note S1.3), which is a conservative estimate of the fidelity of $\mathcal{F} = 95.3(1.2)\%$ obtained via quantum state tomography (detailed in Note S2.1).

Tomography also allows us to visualize the Wigner sphere at each step of the process (Figures 3B–3D). The plot of the violating state $|\mathrm{cat}_{7/2}\rangle_z$ (Figure 3C) shows that it exhibits an interference pattern, which is read out by rotating the axis initially along $\hat{I}_x$ to the $\hat{I}_z$ direction (Figure 3D), and is thereby equivalent to a measurement in the x-basis.

This interference pattern is not only a typical signature of quantum effects but it also provides a qualitative explanation of the quantum score. Figure 3H is key to understanding the physics behind the protocol. As the cat state rotates by an angle φ through the uniform precession, the populations of the $|m_x\rangle$ eigenstates oscillate with $d - 1 = 7$ periods over a 2π rotation. However, the I_x expectation value remains identically zero at all times; this is what would be measured in a standard precession experiment with inductive detection. Conversely, the positivity $\mathrm{Pos}(\hat{I}_x)$, obtained by summing the probabilities of the states with $\hat{I}_x > 0$, is not constant. Taking the cut along the orange dashed line in Figure 3H shows that the spin is more likely to be in the $I_x > 0$ sector, whereas the pattern reverses shortly thereafter.

Figure 3I shows how to break the classical bound using the $|\mathrm{cat}_{7/2}\rangle_z$ state. We sample the precession at the 7 values of φ where the oscillation pattern in $\mathrm{Pos}(\hat{I}_x)$ is at its maximum. The oscillating pattern itself arises from the quantum interference of the $|\pm 7/2\rangle$ states that are superimposed to form the Schrödinger cat states, a pattern that cannot be present for a classical gyroscope. In fact, obtaining $\mathbf{P}_K^d > \mathbf{P}_K^c$ with $K = 7$ also certifies our system to be a qudit with dimension $d \geq 8$, as it is known that no violation of the classical bound is possible when $d \leq K$.[17]

Breaking the bound with smaller spins

To demonstrate the versatility of the protocol, we applied it to smaller dimensional subspaces of the ^{123}Sb nuclear spin, showing that we can break the corresponding classical bound for each even dimension as long as $d > 3$. By focusing on even-dimensional subspaces, we effectively emulate smaller fermionic spins, such as the $I = 3/2$ spin represented by the subspace spanned by $\{|-3/2\rangle, |-1/2\rangle, |1/2\rangle, |3/2\rangle\}$.[30]

Adapting the precession protocol to these subspaces requires slight modifications to the initialization, precession, and basis rotation steps in the pulse sequence. In the initialization step, we generate subspace cats for $d = 8$, 6, and 4 using the ladder initialization method, as described in Figure 2C, and restrict the process to the respective subspaces (Figures 4D–4F). During the uniform precession step, we shift only the relevant $d - 1$ clock phases in the subspace by φ to achieve a virtual $R_z^d(\varphi)$ rotation (detailed in supplemental methods, section 4). Finally, the basis rotation $R_{-y}^d(\pi/2)$ in the subspace is performed by rescaling the drive amplitudes, ensuring the driving strength, determined by $B_{1,i}$ and the spin-7/2 operator element $\hat{I}_x^8$, matches the spin operator in the subspace $\hat{I}_x^d$ (see supplemental methods, section 4 for more details).

Figure 4 shows the results of the protocol applied to these subspaces. The data illustrate how the protocol successfully breaks the classical bound for each tested even dimension.

Maximizing the quantum score with unequal intervals

Finally, we performed a slightly modified version of the protocol to maximize the gap between the classical score and the quantum score, as displayed in Figure 5. In the modified protocol, we loosen the restriction that the K measurement angles must be equally separated. Instead, the measurement angles $\varphi_{\tilde{k}}$ follow the rule $\forall \tilde{k} : |\varphi_{\tilde{k}} - 2\pi\tilde{k}/\tilde{K}| \leq \pi/(2\tilde{K})$, where we note the variables in the modified protocol $(\tilde{k}, \tilde{K})$ with a tilde. Importantly, the loosened restriction leaves the classical bound unchanged,

Please cite this article in press as: Vaartjes et al., Certifying the quantumness of a nuclear spin qudit through its uniform precession, Newton (2025), https://doi.org/10.1016/j.newton.2025.100017

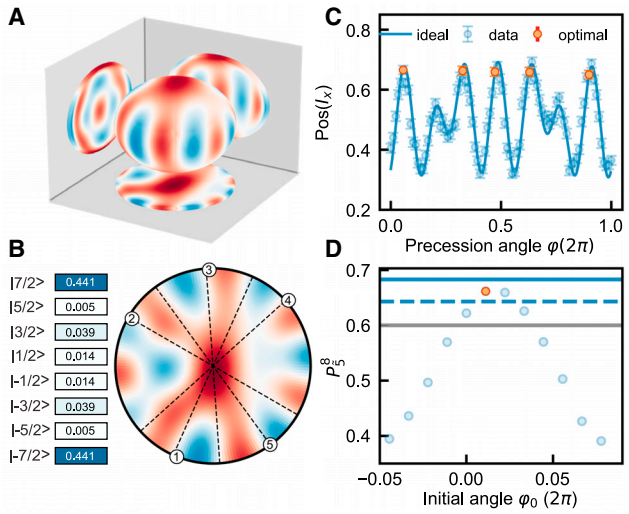

Figure 5. Breaking the classical bound in the modified protocol, with $\tilde{K}$ unevenly spaced angles

(A) Spin-Wigner function of the $|P_5^8\rangle$ state.

(B) Population distribution (bars at left) and polar projection of the Wigner function (right), with the numbered dots indicating the unequally spaced angles $\varphi_{\tilde{k}}$.

(C) The expectation value of Pos($\hat{I}_x$) displays 5 distinct peaks in the data. The orange data points show the optimal set of $\tilde{K} = 5$ unequally separated angles.

(D) The quantum score of the modified protocol P_5^8 as a function of the initial angle φ_0, while keeping the relative separation between the sampled angles fixed. The quantum score in the modified protocol $P_5^8 = 0.662$ (orange dot) reaches beyond the maximum score in the original protocol (blue dashed line) and maximizes the gap to the classical score (gray line). The solid blue line indicates the theoretical maximum score.

but it allows for larger quantum scores for more complicated states.

For example, the state that obtains a larger violation of the classical bound for $d = 8$ and $\tilde{K} = 5$ is given by:

$$|P_5^8\rangle = 0.665|-7/2\rangle + 0.072|-5/2\rangle - 0.199|-3/2\rangle + 0.117|-1/2\rangle - 0.117|1/2\rangle + 0.199|3/2\rangle + 0.072|5/2\rangle - 0.665|7/2\rangle, \quad \text{(Equation 10)}$$

using the set of angles $\{\varphi_k\} = \{-\varphi_1, -\varphi_0, 0, \varphi_0, \varphi_1\}$, where $\varphi_0 = 0.305\pi$ and $\varphi_1 = 0.850\pi$.

The violating states were found by performing gradient descent on max $P_{\tilde{K}}^d$ over the probing angles $\{\varphi_k\}_{\tilde{K}}$ for a selection of initial angles that cover the parameter space. The states for $\tilde{K} = 3$ are known to achieve the global optimal,[37] while the states for $\tilde{K} = 5$ are those that achieve the largest local maxima we found. Both the derived analytical expression for the gradient and details about the optimization can be found in Note S1.4.

DISCUSSION

In this work, we successfully certified quantumness in the time evolution of an 8-dimensional nuclear qudit through its spin precession. Our results show a violation of the classical bound for various sized subspaces and measurement intervals, summarized in Table 1 (detailed protocol data and quantum state tomography data are available in Note S2.3).

Our observation of quantumness in a spin precession may seem at odds with Ehrenfest's theorem. However, in reality, two conditions must be met for Ehrenfest's theorem to yield classical-like dynamics: the Hamiltonian must be up to quadratic in the canonical variables or equivalently linear in angular momenta, and the measured observable must have canonical commutation relations with the Hamiltonian.[38] In our case, while we indeed generated a linear $\hat{I}_z$ Hamiltonian, we measured the positivity operator Pos($\hat{I}_x$), which does not obey the commutation relationships with $\hat{I}_z$ that would make it behave classically. This choice of observable allows for a deviation from classical behavior if the wavefunction of the precessing system is not concentrated in a single region in phase space.[38] Conversely, if one were to measure $\hat{I}_x$ or $\hat{I}_y$ directly—as is done, for example, in ensemble spin resonance experiments with inductive detection—no deviation from classical behavior would be found. Furthermore, in the case of Schrödinger cat states as adopted here, all spin expectation values vanish, yielding zero induction signals; the Ehrenfest theorem would provide the noninsightful result $\partial 0/\partial t = 0$. In fact, we show in Note S1.6 that no deviation will be observed even if the correlations $(\hat{I}_x)^2$ or $\hat{I}_x\hat{I}_y + \hat{I}_y\hat{I}_x$ are measured.

From a foundational perspective, the precession protocol complements other tests of quantumness, such as Bell tests,[9] contextuality experiments,[10] and tests on the reality of the wavefunction.[39] Bell tests primarily probe nonlocality, and contextuality tests examine the incompatibility of classical variables with quantum measurements. The precession protocol is more like the latter in that they both falsify the existence of an underlying ontological model with a classical probability distribution that simply "reveals" the measured observables. However, they differ in assumptions: the precession protocol assumes that the measured observables follow a certain dynamics, while contextuality experiments assume that the measured observables are compatible and thus commuting.

The measured score of $P_3^4 = 0.744(9)$ obtained in our experiment with the spin-3/2 is very close to the general theory-independent bound of $\mathbf{P}_3^G = 0.75$.[24] As this bound is saturated by quantum theory, we have effectively ruled out any alternatives to quantum theory that cannot achieve the same score.

The nonclassical states we have efficiently certified through this protocol are of broad interest for quantum information processing,[19–21,34] quantum sensing,[36] and quantum foundations.[40] The precession protocol adopted here may become a powerful tool for the certification of quantunmess of resource states because it is fairly economical with respect to the type and number of measurements needed. First, in principle, it only requires measuring the sign of the component of the angular momentum along a certain direction. As such, we would not need to resolve the energy level splitting precisely, as long as the splitting between the positive and negative values is large enough to be distinguished. Second, the precession protocol

Please cite this article in press as: Vaartjes et al., Certifying the quantumness of a nuclear spin qudit through its uniform precession, Newton (2025), https://doi.org/10.1016/j.newton.2025.100017

Table 1. Summary of experimental results for different size subspaces d = 8, 6, and 4

State	K ($\tilde{K}$)	(max.) $\mathbf{P}_{\mathbf{K}}^{\mathbf{c}}$	(meas.) P_K^d	(max.) $\mathbf{P}_{\mathbf{K}}^{\mathbf{d}}$	σ
Spin 7/2 (d = 8)					
$\lvert P_7^8\rangle = \frac{1}{\sqrt{2}}\lvert -7/2\rangle - \frac{1}{\sqrt{2}}\lvert 7/2\rangle$	$K = 7$	0.571	0.636 (7)	0.656	18
$\lvert P_5^8\rangle = \frac{1}{\sqrt{2}}\lvert -7/2\rangle - \frac{1}{\sqrt{2}}\lvert 3/2\rangle$	$K = 5$	0.6	0.627 (8)	0.643	6
$\lvert P_3^8\rangle = \frac{\sqrt{7}}{4}\lvert -7/2\rangle - \frac{1}{\sqrt{2}}\lvert -1/2\rangle + \frac{1}{4}\lvert 5/2\rangle$	$K = 3$	0.667	0.695 (9)	0.698	6
$\lvert P_5^8\rangle = 0.665\lvert -7/2\rangle + 0.072\lvert -5/2\rangle - 0.199\lvert -3/2\rangle + 0.117\lvert -1/2\rangle - 0.117\lvert +1/2\rangle + 0.199\lvert +3/2\rangle + 0.072\lvert +5/2\rangle - 0.665\lvert +7/2\rangle$	$\tilde{K} = 5$ (uneven)	0.6	0.662 (8)	0.683	15
$\lvert P_3^8\rangle = 0.600\lvert -7/2\rangle - 0.145\lvert -5/2\rangle - 0.336\lvert -3/2\rangle - 0.078\lvert -1/2\rangle + 0.078\lvert +1/2\rangle + 0.336\lvert +3/2\rangle + 0.145\lvert +5/2\rangle - 0.600\lvert +7/2\rangle$	$\tilde{K} = 3$ (uneven)	0.667	0.720 (9)	0.745	11
Spin 5/2 (d = 6)					
$\lvert P_5^6\rangle = \frac{1}{\sqrt{2}}\lvert -5/2\rangle - \frac{1}{\sqrt{2}}\lvert +5/2\rangle$	$K = 5$	0.6	0.682 (9)	0.688	18
$\lvert P_3^6\rangle = \frac{1}{\sqrt{2}}\lvert -5/2\rangle - \frac{1}{\sqrt{2}}\lvert +1/2\rangle$	$K = 3$	0.667	0.684(10)	0.698	3
$\lvert P_3^6\rangle = 0.645\lvert -5/2\rangle - 0.119\lvert -3/2\rangle - 0.264\lvert -1/2\rangle - 0.264\lvert +1/2\rangle - 0.119\lvert +3/2\rangle + 0.645\lvert +5/2\rangle$	$\tilde{K} = 3$ (uneven)	0.667	0.715(10)	0.746	9
Spin 3/2 (d = 4)					
$\lvert P_3^4\rangle = \frac{1}{\sqrt{2}}\lvert -3/2\rangle - \frac{1}{\sqrt{2}}\lvert 3/2\rangle$	$K = 3$	0.667	0.744(9)	0.750	17

For each K (evenly spaced protocol) or $\tilde{K}$ (unevenly spaced protocol), we display the optimal state, the measured P_k^d, the classical bound $\mathbf{P}_{\mathbf{K}}^{\mathbf{c}}$, the maximum quantum score $\mathbf{P}_{\mathbf{K}}^{\mathbf{d}}$, and the measured violation in units of the measured P_k^d standard deviation σ. For all combinations of d and K ($\tilde{K}$), we find a violation of the classical bound. The uncertainties in the measured P_K^d represent a 2σ confidence interval.

in principle only requires $K = 7$ measurement directions for a spin-7/2, compared to the 45 directions used for full-state tomography.[19,23]

METHODS

Fabrication

The qudit system used in this experiment is the nucleus of a ^{123}Sb donor, introduced into isotopically enriched ^{28}Si by ion implantation. A 900-nm-thick epilayer of ^{28}Si (730 ppm residual ^{29}Si) was deposited on a natural Si handle wafer. N-type ohmic leads and p-type channel stoppers to prevent leakage currents were formed by thermal diffusion of phosphorus and boron, respectively. A 200-nm-thick SiO_2 field oxide and an 8-nm-thick high-quality SiO_2 gate oxide were grown in oxidation furnaces. $^{123}Sb^+$ ions (18 keV, 5×10^{11} cm^{-2}) were implanted at normal incidence through a 90 × -100 nm implant window in a polymethyl methacrylate mask. A rapid thermal anneal at 1,000° C for 10 s in a nitrogen atmosphere was performed to repair the implantation damage and activate the donors. Surface nanoelectronics were fabricated as standard for our qubit devices using three layers of electron beam lithography and aluminum deposition. Each layer is electrically insulated from the others with native Al_2O_3. Finally, the sample was annealed in forming gas (400° C, 15 min, 95% N_2:5% H_2) to passivate interface traps.

Experimental setup

The device was wire-bonded to a gold-plated printed circuit board and placed in a copper enclosure within a superconducting solenoid generating a 1.384-T magnetic field. The setup was cooled to 18 mK in a Bluefors BF-LD400 dilution refrigerator. Direct current (DC) voltages were applied on the electrostatic gates with SRS SIM928 sources. The donor gates used for fast pulsing used a room temperature resistive power combiner. The alternating current component on the gates was generated using a Quantum Machines OPX+ and filtered with an 80-MHz low-pass filter. Signals on the DC gates were filtered with a 20-Hz low-pass filter. All filtering occurred at the mixing chamber plate, with graphite-coated coaxial cables. Electron spin resonance (ESR) transitions were induced using a Keysight E8267D PSG microwave source (38.94269 GHz carrier frequency) with single-sideband modulation. The lower-frequency (around 7 MHz) NMR pulses were generated by the OPX+. The ESR and NMR signals were combined before going into the refrigerator by a Marki Microwave DPX-1721 diplexer. The single electron transistor (SET) current was amplified by a Femto DLPCA-200, SRS SIM910 before being filtered by an SRS SIM965 and digitized via the OPX+.

RESOURCE AVAILABILITY

Lead contact

Requests for further information and resources should be directed to and will be fulfilled by the lead contact, Andrea Morello (a.morello@unsw.edu.au).

Materials availability

This study did not generate new materials.

Data and code availability

- The measured raw data have been deposited in the online Dryad repository at https://doi.org/10.5061/dryad.547d7wmj0 and are publicly available as of the date of publication.
- All original code to analyze the raw data is publicly available at https://doi.org/10.5061/dryad.547d7wmj0.
- Any additional information required to reanalyze the data reported in this paper is available from the lead contact upon request.

ACKNOWLEDGMENTS

The research was funded by an Australian Research Council Discovery Project (grant no. DP-210103769) and the US Army Research Office (contract no. W911NF-23-1-0113). A.M. acknowledges the support of an Australian Research Council Laureate Fellowship (project no. FL-240100181). We acknowledge the facilities and the scientific and technical assistance provided by the University of New South Wales node of the Australian National Fabrication Facility (ANFF), and the Heavy Ion Accelerators (HIA) nodes at the University of Melbourne and the Australian National University. ANFF and HIA are supported by the Australian government through the National Collaborative Research Infrastructure Strategy (NCRIS) program. Ion beam facilities employed by D.N.J. and A.M.J. were co-funded by the Australian Research Council Centre of Excellence for Quantum Computation and Communication Technology (grant no. CE170100012). X.Y., B.W., M.R.v.B., and A.V. acknowledge support from the Sydney Quantum Academy. D.N.J. acknowledges the support of a Royal Society Wolfson Visiting Fellowship RSWVF/211016. L.H.Z. and V.S. are supported by the National Research Foundation, Singapore, and A*STAR under its CQT Bridging grant. N.A. is a KBR employee working under the Prime Contract no. 80ARC020D0010 with the National Aeronautics and Space Administration (NASA) Ames Research Center and is grateful for the collaborative agreement between NASA and Centre for Quantum Computation and Communication Technology (CQC2T). The US government retains, and by accepting the article for publication, the publisher acknowledges that the US government retains, a nonexclusive, paid-up, irrevocable, worldwide license to publish or reproduce the published form of this work, or allow others to do so, for US government purposes. Sandia National Laboratories is a multi-program laboratory managed and operated by National Technology and Engineering Solutions of Sandia LLC, a wholly owned subsidiary of Honeywell International, for the US Department of Energy's National Nuclear Security Administration under contract DE-NA-0003525. All statements of fact, opinion, or conclusions contained herein are those of the authors and should not be construed as representing the official views or policies of the US Department of Energy or the US government.

AUTHOR CONTRIBUTIONS

Conceptualization: A.V., M.N., L.H.Z., B.W., X.Y., D.H., D.S., A.K., M.R.v.B., N.A., V.S., and A.M. Investigation: A.V. and M.N. Methodology: A.V., M.N., L.H.Z., B.W., X.Y., D.H., D.S., A.K., M.R.v.B., R.J.M., R.B.-K., and N.A. Resources: D.H., A.M.J., F.E.H., K.M.I., D.N.J., and A.M. Software: A.V., M.N., B.W., X.Y., and M.R.v.B. Writing—original draft: A.V., M.N., L.H.Z., V.S., and A.M. Writing—review & editing: B.W., X.Y., D.H., D.S., A.K., M.R.v.B., R.B.-K., and N.A. Supervision: A.S.D., D.N.J., V.S., and A.M. Funding acquisition: D.N.J., V.S., and A.M.

DECLARATION OF INTERESTS

A.M. is an inventor on a patent related to this work, describing the use of high-spin donor nuclei as quantum information processing elements (application no. AU2019227083A1, US16/975,669, WO2019165494A1). A.S.D. is the chief executive officer and a director of Diraq Pty. Ltd. F.E.H. and A.S.D. declare equity interest in Diraq Pty. Ltd. A.M. is an advisory board member of the journal *Newton*.

DECLARATION OF GENERATIVE AI AND AI-ASSISTED TECHNOLOGIES

During the preparation of this work, the authors used Perplexity to find relevant literature and to improve the language of the manuscript through finding synonyms. After using this tool/service, the authors reviewed and edited the content as needed and take full responsibility for the content of the published article.

SUPPLEMENTAL INFORMATION

Supplemental information can be found online at https://doi.org/10.1016/j.newton.2025.100017.

Received: October 10, 2024
Revised: November 29, 2024
Accepted: January 22, 2025
Published: February 14, 2025

REFERENCES

1. Ehrenfest, P. (1927). Bemerkung über die angenäherte Gültigkeit der klassischen Mechanik innerhalb der Quantenmechanik. Z. Phys. *45*, 455–457. https://doi.org/10.1007/BF01329203.
2. Slichter, C.P. (1990). Principles of Magnetic Resonance, Vol. 1 of Springer Series in Solid-State Sciences (Springer). https://doi.org/10.1007/978-3-662-09441-9.
3. Arecchi, F.T., Courtens, E., Gilmore, R., and Thomas, H. (1972). Atomic Coherent States in Quantum Optics. Physiol. Rev. *6*, 2211–2237. https://doi.org/10.1103/PhysRevA.6.2211.
4. Kitagawa, M., and Ueda, M. (1993). Squeezed spin states. Phys. Rev. *47*, 5138–5143. https://doi.org/10.1103/PhysRevA.47.5138.
5. Bell, J.S. (1966). On the Problem of Hidden Variables in Quantum Mechanics. Rev. Mod. Phys. *38*, 447–452. https://doi.org/10.1103/RevModPhys.38.447.
6. Gleason, A. (1957). Measures on the Closed Subspaces of a Hilbert Space. Indiana Univ. Math. J. *6*, 885–893.
7. Kochen, S., and Specker, E. (1967). The Problem of Hidden Variables in Quantum Mechanics. Indiana Univ. Math. J. *17*, 59–87.
8. Mermin, N.D. (1993). Hidden variables and the two theorems of John Bell. Rev. Mod. Phys. *65*, 803–815. https://doi.org/10.1103/RevModPhys.65.803.
9. Bell, J.S. (1964). On the Einstein Podolsky Rosen paradox. Physics Physique Fizika *1*, 195–200. https://doi.org/10.1103/PhysicsPhysiqueFizika.1.195.
10. Leggett, A.J., and Garg, A. (1985). Quantum mechanics versus macroscopic realism: Is the flux there when nobody looks? Phys. Rev. Lett. *54*, 857–860. https://doi.org/10.1103/PhysRevLett.54.857.
11. Barrett, J., and Kent, A. (2004). Non-contextuality, finite precision measurement and the Kochen–Specker theorem. Stud. Hist. Philos. Sci. B Stud. Hist. Philos. Mod. Phys. *35*, 151–176. https://doi.org/10.1016/j.shpsb.2003.10.003.
12. Kleinmann, M., Gühne, O., Portillo, J.R., Larsson, J.Å., and Cabello, A. (2011). Memory cost of quantum contextuality. New J. Phys. *13*, 113011. https://doi.org/10.1088/1367-2630/13/11/113011.
13. Wilde, M.M., and Mizel, A. (2012). Addressing the Clumsiness Loophole in a Leggett-Garg Test of Macrorealism. Found. Phys. *42*, 256–265. https://doi.org/10.1007/s10701-011-9598-4.
14. Kenfack, A., and Życzkowski, K. (2004). Negativity of the Wigner function as an indicator of non-classicality. J. Opt. B Quantum Semiclassical Opt. *6*, 396–404. https://doi.org/10.1088/1464-4266/6/10/003.
15. Davis, J., Kumari, M., Mann, R.B., and Ghose, S. (2021). Wigner negativity in spin- j systems. Phys. Rev. Res. *3*, 033134. https://doi.org/10.1103/PhysRevResearch.3.033134.

16. Tsirelson, B. (2006). How often is the coordinate of a harmonic oscillator positive?. Preprint at arXiv. https://doi.org/10.48550/arXiv.quant-ph/0611147.

17. Zaw, L.H., Aw, C.C., Lasmar, Z., and Scarani, V. (2022). Detecting quantumness in uniform precessions. Phys. Rev. *106*, 032222. https://doi.org/10.1103/PhysRevA.106.032222.

18. Aravinda, S., Srikanth, R., and Pathak, A. (2017). On the origin of nonclassicality in single systems. J. Phys. Math. Theor. *50*, 465303. https://doi.org/10.1088/1751-8121/aa8d29.

19. Yu, X., Wilhelm, B., Holmes, D., Vaartjes, A., Schwienbacher, D., Nurizzo, M., Kringhøj, A., van Blankenstein, M.R., Jakob, A.M., Gupta, P., and Hudson, F.E. (2025). Creation and manipulation of Schrödinger cat states of a nuclear spin qudit in silicon. Nat. Phys. https://doi.org/10.1038/s41567-024-02745-0.

20. Champion, E., Wang, Z., Parker, R., and Blok, M. (2024). Multi-frequency control and measurement of a spin-7/2 system encoded in a transmon qudit. Preprint at arXiv. https://doi.org/10.48550/arXiv.2405.15857.

21. Roy, S., Senanian, A., Wang, C.S., Wetherbee, O.C., Zhang, L., Cole, B., Larson, C.P., Yelton, E., Arora, K., McMahon, P.L., et al. (2024). Synthetic high angular momentum spin dynamics in a microwave oscillator. Preprint at arXiv. https://doi.org/10.48550/arXiv.2405.15695.

22. Hofmann, H.F., and Takeuchi, S. (2004). Quantum-state tomography for spin-*I* systems. Phys. Rev. *69*, 042108. https://doi.org/10.1103/PhysRevA.69.042108.

23. Perlin, M.A., Barberena, D., and Rey, A.M. (2021). Spin qudit tomography and state reconstruction error. Phys. Rev. *104*, 062413. https://doi.org/10.1103/PhysRevA.104.062413.

24. Zaw, L.H., Weilenmann, M., and Scarani, V. (2024). A theory-independent bound saturated by quantum mechanics. Preprint at arXiv. https://doi.org/10.48550/arXiv.2401.16147.

25. Gupta, P., Vaartjes, A., Yu, X., Morello, A., and Sanders, B.C. (2024). Robust macroscopic Schrödinger's cat on a nucleus. Phys. Rev. Res. *6*, 013101. https://doi.org/10.1103/PhysRevResearch.6.013101.

26. Asaad, S., Mourik, V., Joecker, B., Johnson, M.A.I., Baczewski, A.D., Firgau, H.R., Mądzik, M.T., Schmitt, V., Pla, J.J., Hudson, F.E., et al. (2020). Coherent electrical control of a single high-spin nucleus in silicon. Nature *579*, 205–209. https://doi.org/10.1038/s41586-020-2057-7.

27. Fernández de Fuentes, I., Botzem, T., Johnson, M.A.I., Vaartjes, A., Asaad, S., Mourik, V., Hudson, F.E., Itoh, K.M., Johnson, B.C., Jakob, A.M., et al. (2024). Navigating the 16-dimensional Hilbert space of a high-spin donor qudit with electric and magnetic fields. Nat. Commun. *15*, 1380. https://doi.org/10.1038/s41467-024-45368-y.

28. Leuenberger, M.N., and Loss, D. (2003). Grover algorithm for large nuclear spins in semiconductors. Phys. Rev. B *68*, 165317. https://doi.org/10.1103/PhysRevB.68.165317.

29. Godfrin, C., Ferhat, A., Ballou, R., Klyatskaya, S., Ruben, M., Wernsdorfer, W., and Balestro, F. (2017). Operating Quantum States in Single Magnetic Molecules: Implementation of Grover's Quantum Algorithm. Phys. Rev. Lett. *119*, 187702. https://doi.org/10.1103/PhysRevLett.119.187702.

30. Neeley, M., Ansmann, M., Bialczak, R.C., Hofheinz, M., Lucero, E., O'Connell, A.D., Sank, D., Wang, H., Wenner, J., Cleland, A.N., et al. (2009). Emulation of a Quantum Spin with a Superconducting Phase Qudit. Science *325*, 722–725. https://doi.org/10.1126/science.1173440.

31. Cybenko, G. (2001). Reducing quantum computations to elementary unitary operations. Comput. Sci. Eng. *3*, 27–32. https://doi.org/10.1109/5992.908999.

32. Puri, S., St-Jean, L., Gross, J.A., Grimm, A., Frattini, N.E., Iyer, P.S., Krishna, A., Touzard, S., Jiang, L., Blais, A., et al. (2020). Bias-preserving gates with stabilized cat qubits. Sci. Adv. *6*, eaay5901. https://doi.org/10.1126/sciadv.aay5901.

33. Gross, J.A. (2021). Designing Codes around Interactions: The Case of a Spin. Phys. Rev. Lett. *127*, 010504. https://doi.org/10.1103/PhysRevLett.127.010504.

34. Gross, J.A., Godfrin, C., Blais, A., and Dupont-Ferrier, E. (2024). Hardware-efficient error-correcting codes for large nuclear spins. Phys. Rev. Appl. *22*, 014006. https://doi.org/10.1103/PhysRevApplied.22.014006.

35. Facon, A., Dietsche, E.K., Grosso, D., Haroche, S., Raimond, J.M., Brune, M., and Gleyzes, S. (2016). A sensitive electrometer based on a Rydberg atom in a Schrödinger-cat state. Nature *535*, 262–265. https://doi.org/10.1038/nature18327.

36. Chalopin, T., Bouazza, C., Evrard, A., Makhalov, V., Dreon, D., Dalibard, J., Sidorenkov, L.A., and Nascimbene, S. (2018). Quantum-enhanced sensing using non-classical spin states of a highly magnetic atom. Nat. Commun. *9*, 4955. https://doi.org/10.1038/s41467-018-07433-1.

37. Zaw, L.H., and Scarani, V. (2024). All three-angle variants of tsirelson's precession protocol, and improved bounds for wedge integrals of wigner functions. Preprint at arXiv. https://doi.org/10.48550/arXiv.2411.03132.

38. Hall, B.C. (2013). Quantum Theory for Mathematicians Vol. 267 of *Graduate Texts in Mathematics* (Springer). https://doi.org/10.1007/978-1-4614-7116-5.

39. Ringbauer, M., Duffus, B., Branciard, C., Cavalcanti, E.G., White, A.G., and Fedrizzi, A. (2015). Measurements on the reality of the wavefunction. Nat. Phys. *11*, 249–254. https://doi.org/10.1038/nphys3233.

40. Fröwis, F., Sekatski, P., Dür, W., Gisin, N., and Sangouard, N. (2018). Macroscopic quantum states: Measures, fragility, and implementations. Rev. Mod. Phys. *90*, 025004. https://doi.org/10.1103/RevModPhys.90.025004.